

# Microvoids in Solids: Synchrotron Radiation Phase Contrast Imaging and Simulations

Victor G. Kohn, Tatiana S. Argunova,\* and Jung Ho Je

Phase contrast imaging study and computer simulations of microvoids located in solid materials of complex structure have been reported. Images of microvoids arise as interference fringes due to coherent scattering of synchrotron radiation (SR) in matter. In the first part of this work, the simulation of the experimental image of a single tubular microvoid in a SiC crystal to illustrate the advantages and limitations of one-dimensional (1D) phase-contrast method and to discuss the approach to 2D objects has been performed. In the second part, a new iterative method for the variable wave function of radiation is employed to examine the applicability of the phase-contrast method for an array of tubules. The latter method has been shown to be sufficiently accurate to be useful when a number of tubules along the beam is limited. Finally, the interference patterns generated by waves passing through a phantom dentin specimen have been calculated and analyzed. It has been demonstrated that both methods have extensive possibilities to determine the period in the lattice of tubules, even in the presence of some disorder.

Since 1995, more than 1000 papers have been published by various workers using this technique (see, e.g., reviews [3,4]). Among them, there have been many reports on experiments only. Meanwhile, there is an acute need to develop techniques for obtaining quantitative information from image data. There are two ways to work out the inverse problem of the phase determination: computer simulations and direct phase retrieval. Even the first study<sup>[1]</sup> had already reported on the computer simulations. Later this approach was used to optimize experimental parameters (see, e.g., refs. [5,6]) or to investigate materials and objects, some of which are similar to those used for this study.<sup>[7,8]</sup> On the other hand, various procedures have been developed for the retrieval of phase maps (see, e.g., refs. [9–11]). Owing to them, the phase determination is now routinely used to obtain real-space parameters of materi-

als.<sup>[12]</sup> Further development of quantitative imaging is of special theoretical and practical interests.

There are three kinds of phase-contrast images which depend on the sample-to-detector distance. Near-field images are obtained at short distances. Far-field images are obtained at large distances, and Fresnel images are obtained at intermediate distances, where the diameter of the first Fresnel zone is comparable with the transverse size of the object. Available reports on the quantitative phase determination mainly contain experimental images recorded in the near-field of the specimen. Such data can be interpreted on the basis of the quasi-geometrical optics approach which is only weakly sensitive to the spatial and temporal coherence of X-ray radiation. It should be noted that these studies have not addressed objects of relatively small transverse size. For instance, the image of a micrometer-sized cavity acquired with an effective pixel size slightly less than a micrometer will not show discernible details in the near field. In the far field the image will have a larger size, but a lower count rate (intensity) in the same period of time. The intensity can be increased by using a pink beam of relative bandwidth  $\approx 0.1$ . A great loss of monochromaticity will, however, lead to a significant reduction of the contrast to a value less than 1%. Under these conditions, the phase-retrieval methods based on the Maxwell equation for a coherent beam face a serious problem.

Nevertheless, it is still possible to fit the images and determine the size of micro-objects via computer simulations. Starting with a certain model of an object with several parameters, we

## 1. Introduction

Solid materials may contain inhomogeneities, such as microcracks, micropipes, minute cavities and pores. Despite the small size, they can be detected using synchrotron radiation (SR). A thickness variation of a few micrometers, for instance associated with a cavity within the material, can produce a noticeable phase shift of the coherent SR beam. This leads to curving the surfaces of constant phase, and, at some distance from the specimen, to an inhomogeneous distribution of intensity that can be revealed through the phase-contrast technique pioneered date back to the mid-1990s.<sup>[1,2]</sup>

Dr. V. G. Kohn  
National Research Centre 'Kurchatov Institute'  
1 Kurchatov sq., 123182 Moscow, Russia

Dr. T. S. Argunova  
Ioffe Institute  
RAS  
Polytekhnicheskaya st. 26, 194021 St. Petersburg, Russia  
E-mail: argunova\_t@yahoo.com

Prof. J. H. Je  
Department of Materials Science and Engineering  
Pohang University of Science and Technology  
San 31 Hyoja-dong, Namku, 790-784 Pohang, Republic of Korea

 The ORCID identification number(s) for the author(s) of this article can be found under <https://doi.org/10.1002/pssb.201800209>.

DOI: 10.1002/pssb.201800209

determine the real parameters when we arrive at the best match to the experiment. Kohn et al.<sup>[13–16]</sup> have developed 1D and 2D simulation techniques which have the essential advantage of providing summation over the spectrum. The fitting procedures use standard approximations. In particular, the change in the trajectory of X-rays within the object is neglected, and the wave function acquires a phase shift and a change in amplitude due to changes in the electron density and absorption. The methods were applied to microvoids in a crystalline matrix.

Unlike single crystals in which voids are relatively sparse, some materials, e.g., biocomposites, such as bone tissues or dentin, can contain dense arrays of voids that are proven to play a significant role in toughening.<sup>[17,18]</sup> At present, microstructure of biocomposites is of great interest. The reason for the interest is that they promise great potential for medical, tissue engineering, and bioinspired applications. Dentin contains a lattice of well-ordered or quasi-ordered tubules. Despite the extensive structural information obtained by other methods (e.g., SEM, TEM, AFM, etc.), it is still the question of how the dentinal tubules are arranged in space. To clarify this problem, it may be interesting to explore the possibilities of the non-destructive phase-contrast technique<sup>[1,2]</sup> in combination with computer simulations. This could prove advantageous compared to the other SR methods.<sup>[7,19]</sup> However, the summation of the phase shift, produced by a single tubule, along the X-ray trajectory that is assumed to be unchanged may be inaccurate because the perturbation of the wave-function in fact occurs over the entire volume of a relatively large specimen. We are unaware of a work that would account for a variable wave function of radiation.

The aim of this work is to develop a more accurate approach that offers a solution to the problem of computer simulations of images of complex biomaterials. We generate simple model systems of multiple tubules. Then we calculate the interference patterns and compare the results of the phase-contrast method with those of the new iterative method for the variable wave function of radiation. This allows us to determine the applicability of the phase contrast method. Next we apply the phase contrast method to study the variation in the image of a phantom dentin specimen with the distance from the specimen to detector.

We begin with a brief example of a tubular void in a single crystal to show the principles of simulating the images of 1D objects. This is followed by a description of the basics of simulating the images of 2D objects, represented by more complex model systems of tubules.

## 2. A Tubular Void in a Single Crystal

### 2.1. 1D Simulation Program and Theory

Voids in solids produce strong variations of the electron density, which allows to image them using phase contrast methods. Let the material density vary in two directions, i.e., along and across the beam, and let a coordinate  $x$  be directed across the beam. In the phase-contrast method, an object is described by the transmission function  $T(x)$ , which is the ratio of the wave function of radiation directly behind the real object (i.e., with

voids) to the wave function of the ideal object (i.e., without voids). Since we neglect the deviation of the ray trajectories inside the object, the transmission function can be represented by the exponent

$$T(x) = \exp(iK \eta t(x)) \quad (1)$$

where  $K = 2\pi/\lambda = (2\pi/hc)E$  is the modulus of the wave vector of monochromatic radiation,  $\lambda$  is the wavelength,  $E$  is the photon energy,  $h$  is the Planck's constant,  $c$  is the velocity of light,  $\eta = \delta - i\beta = 1 - n$  ( $n$  is the complex refractive index of the material around the voids),  $t(x)$  is the variable thickness of the material in the path of the beam passing through the point  $x$ , with account of the voids.

In fact,  $t(x)$  is the thickness of the voids; for this reason, the exponential argument has a plus sign. That is, the phase in the void becomes larger in comparison with the material. The same holds for the amplitude. In this model, the density is assumed to be homogeneous everywhere, except for the voids in which the material is absent. If the material has an inhomogeneous density, then one can say that the voids have an effective thickness.

In crystals, single voids are usually observed. We are interested in cylindrical voids with an elliptical cross-section in which  $D_0$  is the longitudinal diameter (along the beam),  $D$  is the transverse diameter (across the beam). In this case

$$t(x) = D_0(1 - x^2/R^2)^{1/2} \theta(R - |x|) \quad (2)$$

where  $R = D/2$ . Here  $\theta(x)$  is Heaviside function where  $\theta(x) = 1$  for  $x > 0$  and  $\theta(x) = 0$ , otherwise.

If the object has small transverse dimensions, then the incident wave can be considered as a plane wave. The account of a spherical wave front only leads to scaling of the longitudinal and transverse coordinates but does not change the image structure on the merits.<sup>[16]</sup> At some distance  $z$  from the object, the phase contrast is determined by the integral that is the convolution of the transmission function  $T(x)$  with the Fresnel propagator

$$P(x, z) = \frac{1}{(i\lambda z)^{1/2}} \exp\left(i\pi \frac{x^2}{\lambda z}\right) \quad (3)$$

We note that it is convenient to perform numerical calculations for the integral with finite limits and for a relative change in intensity, namely

$$\frac{\Delta I(x)}{I_0} = |A(x)|^2 - 1 \quad (4)$$

where

$$A(x) = 1 + \int dx' P(x - x', z)[T(x) - 1] \quad (5)$$

In this case, the distance is counted from the middle of the longitudinal thickness of the object, although the thickness itself is not included in the result of the calculation.

Computer simulations were performed with the FIMTIM (Fit Micro-Tube Image) program.<sup>[14]</sup> The program was originally designed to simulate pink beam images by summing the images for monochromatic harmonics with a weight corresponding to the real spectrum measured by a detector. FIMTIM can estimate the real spectrum, taking into account all the absorbers on the beam path. The program also allows one to simulate a monochromatic image. Below we illustrate how the program can be used to fit images of tubular voids.

FIMTIM starts the simulation by reading the experimental intensity profile measured across the void axis, then calculates the theoretical profiles for some trial parameters of the cross-section. The goal of the simulation is to find the transverse  $D$  and longitudinal diameters  $D_0$  using only one projection image. In the search for the best match, the program automatically varies the diameters and finds the sum  $\chi^2(D, D_0)$  of least squared deviations on the certain set of points with the certain step using the effective algorithm. To estimate the accuracy, FIMTIM can draw a map of  $\chi^2 - \chi_{\min}^2$  as a function of  $D, D_0$  near the minimum point.

## 2.2. Experimental Section

The Pohang Light Source (PLS), Pohang city, Republic of Korea, is operated with full electron energy of 3 GeV. PLS is housing imaging beamlines at the bending magnet ports and the biomedical-imaging beamline at a multipole wiggler port. Since 2013 phase contrast experiments have been performed on the wiggler-beamline which is also dedicated to tomography and topography techniques. The experiments presented in this paper were carried out using the photon fluxes from a bending magnet and from a wiggler at 6D and 6C beamlines, respectively. On the bending-magnet beamline there were no optical components between the source (having the size  $160 \text{ (H)} \times 60 \text{ (V)} \mu\text{m}^2$ ) and the specimen, located at a distance of 32 m from the source. The large source-to-specimen distance  $L$  and the small source size in the vertical direction  $S$  resulted in the lateral coherence length  $L_c = \lambda/2a = 21 \mu\text{m}$ , where  $\lambda = 0.775 \text{ \AA}$  is the wavelength for the photon energy  $E = 16 \text{ keV}$ , and  $a = S/L$  is the angular size of the source as seen from a point in the specimen.

The pink beam spectrum was formed due to the presence of absorbers on the beam path, which were the 2-mm-thick Be window and the specimen. The latter was a SiC plate with a thickness of  $\approx 500 \mu\text{m}$ . The detector placed behind the specimen measured a well-pronounced spectrum maximum with an effective full width at half height  $\Delta E = 11 \text{ keV}$ . The temporal coherence was estimated as 1.2 Å.

The specimens were cut out from the 6H-SiC crystal grown by the sublimation method along the  $\langle 11\bar{2}0 \rangle$  direction. In the  $a$ -face growth (see, e.g., ref. [20]), micropipes, which represent hollow cores of screw superdislocations, are not formed. Prior to growth, a grooved relief ( $500 \mu\text{m}$  spacing,  $50\text{--}80 \mu\text{m}$  width and depth) was excised on the  $a$ -plane surface of the SiC seed with a diamond saw. The seed surface was etched by molten KOH. The relief was made for the purpose of controlling the density of dislocations that propagated into the crystal from the seed. The growth process was carried out in an Ag atmosphere under a pressure of 0.01–0.07 bar at a temperature of 2100–2200 °C with

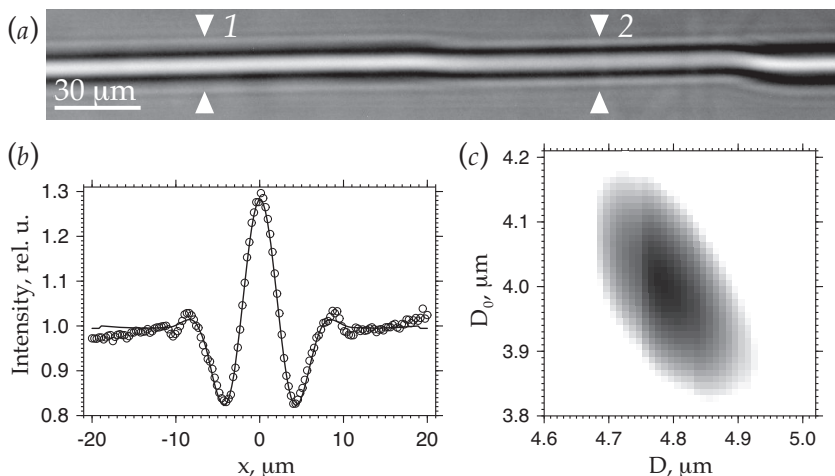
a rate of  $500 \mu\text{m h}^{-1}$ . The grown boule was sliced into (0001) specimens further subjected to grinding and polishing. The thickness of a specimen was  $\approx 50 \mu\text{m}$ . It was found that the boule contained tubular microvoids. Unlike dislocated micropipes, which usually propagated along the (0001) direction, these voids were oriented mainly parallel to the (0001) plane, and they could vary their cross-sections along with their orientation in space.

Figure 1a shows the image of the void registered in the far field. We notice that the void orientation varies slightly. We note that the 1D approach restores the proper diameters only if the cross-section keeps the constant size within the segment longer than  $2r_1$  along the void axis, where  $r_1 = (\lambda z)^{1/2}$  is the radius of the first Fresnel zone. For  $\lambda = 0.775 \text{ \AA}$  and  $z = 40 \text{ cm}$  the diameter is  $2r_1 = 11.10 \mu\text{m}$ . In Figure 1a, noticeable changes along the void axis occur in the segment much longer than this value. The experimental intensity profiles were measured across the axis in the regions indicated by arrows 1 and 2. The normalized experimental curve, measured in region 1, is represented by markers, and the simulated theoretical profile is shown by a solid line in Figure 1b. The best agreement ( $\chi^2 = 1.40 \times 10^{-4}$ ) between the profiles was achieved for the diameters  $D^{(1)} = 4.77 \mu\text{m}$  and  $D_0^{(1)} = 3.99 \mu\text{m}$ .

Can one trust the result of the simulation? In order to estimate the accuracy of the obtained parameters, the FIMTIM program can draw the sum  $\chi^2(D, D_0)$  of least squared deviations near the minimum point as a function of  $D^{(1)}$  and  $D_0^{(1)}$ . Figure 1c shows the black–white contrast map with black color for  $\chi_{\min}^2 = 1.39 \times 10^{-4}$  and white color for  $\chi_{\max}^2 = 1.49 \times 10^{-4}$  or more. One can see that the region of small values of  $\chi^2$  is not localized. This result was theoretically explained by Kohn et al.<sup>[16]</sup> Provided that the image of the microvoid is measured in the far field and, unless the phase shift is less than unity, the detailed structure of the void cross-section can not be revealed. For the void in Figure 1a, the Fraunhofer diffraction condition is fulfilled, since  $D^{(1)} < 2r_1$ . Therefore, the only parameter that can be obtained from the image is the size of the cross-sectional area in region 1:  $\sigma_1 = \pi(D \times D_0)/4 = 15 \mu\text{m}^2$ .

In region 2, the center of the void image darkens, and the transverse dimension decreases along its axis. The change in contrast is caused by changes either in the size of the cross-sectional area, in the cross-section shape, or in both parameters. Here, the best fit ( $\chi^2 = 1.54 \times 10^{-4}$ ) between the simulation and the experiment is obtained for  $D^{(2)} = 2.62 \mu\text{m}$  and  $D_0^{(2)} = 2.82 \mu\text{m}$ . We notice that the cross-sectional area of the void has changed in region 2:  $\sigma_2 = 6 \mu\text{m}^2$ .

The obtained data were insufficient to explain the formation of such voids. Nevertheless, the difference between our samples and those described elsewhere<sup>[20]</sup> should be taken into account. The feature of our samples was the presence of artificial grooves. We suppose that the voids are formed by the vacancy diffusion and coagulation mechanism. When the free surfaces of the grooves appear in the interface region of the growing crystal, the vacancies are able to nucleate not only at the growth front, but also at the faces of the grooves. At the same time, plastic deformation, which occurs during growth, can make attractive lattice sites, e.g., grain and subgrain boundaries, dislocation slip bands, etc. acting as vacancy sinks. It was reported in ref. [20] that crystals grown in the  $[\bar{1}100]$  and  $[11\bar{2}0]$  directions contained edge dislocations, stacking faults, and tilted subgrain boundaries



**Figure 1.** a) Phase-contrast image of a tubular void in the bulk of 6H-SiC crystal. Multilayer monochromator,  $E = 16$  keV,  $z = 40$  cm. Effective pixel size:  $0.28 \mu\text{m}$ . White arrows 1 and 2 indicate the levels at which the simulation is performed. b) The experimental (markers) and theoretical profiles in the case of best coincidence ( $\chi^2 = 1.40 \times 10^{-4}$ ). c) A map showing the sum  $\chi^2$  of least squared deviations as a function of  $D$  and  $D_0$  at level 1.

located in a plane parallel to the growth direction. In our white-beam topography observations, we detected subgrain boundaries and dislocation slip bands located in the (0001) plane parallel to the  $[11\bar{2}0]$  growth direction. The high growth temperature facilitates the migration of vacancies to the sinks. Rough estimate shows that the characteristic rate of the carbon vacancy diffusion is  $\approx 1 \text{ cm h}^{-1}$  at the temperature  $T = 2300 \text{ K}$ , which is much larger than the typical growth rate for our crystal. Therefore, the vacancies seem to have enough time to coagulate and to form the voids along the defective boundaries.

### 3. Computer Simulations of 1D Arrays of Tubules in Dentin

Some materials (e.g., photonic crystals or dentin) contain many voids spaced apart a distance comparable to their transverse dimensions. In this case, the perturbation of the wave function will occur over the entire specimen, whose length can be rather large. The calculation method based on the summation of a phase along an unchanged trajectory (known as the projection approximation) may be inaccurate. It is necessary to take into account the gradual change in the wave function after each void at a distance between them. In order to verify the applicability of the phase-contrast method to such materials, let us consider a simplest model in which a chain of identical voids, spaced by a distance of  $p$ , is parallel to the beam trajectory. Assume that the cross section of a void is elliptical in shape with the diameters  $D_0$  and  $D$ , and the number of such voids is  $N$ . We are interested in the image of such object at a variable distance  $Z$  from its end. In the phase contrast method we use the same formulas (1)–(4) as before, but instead of  $D_0$  in (2) one must write  $D_0 N$  and use a distance  $z = Z + p(N - 1)/2$ .

We must compare the results of the calculation with a more accurate method. The latter is the iterative method<sup>[21–23]</sup> that uses a variable wave function of radiation  $A_n(x)$ . Its initial value is

equal to unity:  $A_0(x) = 1$ . On each iteration of a loop with  $(N - 1)$  repetitions one calculates the integral

$$A_{n+1}(x) = 1 + \int dx' P(x - x', p) [A_n(x) T(x) - 1] \quad (6)$$

where the function  $T(x)$  is described by the formulas (1) and (2). In the last iteration the parameter  $p$  in (6) is replaced by  $Z$ . Then one calculates the square of the modulus of the function  $A_N(x)$  and subtracts 1.

That is, the iterative method applies the ideas of phase contrast only to a single void; and only for a single void is the change in the complex phase on the beam path calculated. As for the spacing between the voids, it is estimated more accurately, according to the Huygens–Fresnel principle. It is known that the Fresnel propagator is almost equal to a delta function at short distances. If the Fresnel propagator is replaced with a delta function, we at once obtain an analogue of the first calculation method without taking into account half the thickness of the specimen. However, even if the distance is small, the Fresnel propagator is not quite equal to delta function; and when the number  $N$  of voids is large enough, the result of the iterative method should be somewhat different from that of the phase-contrast method. The very fact that there are differences in the results of the two methods means that the phase-contrast method is inapplicable.

The calculations were performed by the two methods for dentin material and the photon energy  $E = 12 \text{ keV}$ . It was assumed that  $D_0 = D = 4 \mu\text{m}$  and  $p = 10 \mu\text{m}$ . We have calculated the complex refractive index of dentin taking into account that  $\approx 50\%$  of its volume is occupied by calcium hydroxyapatite, which has the chemical formula  $\text{Ca}_5\text{P}_3\text{O}_{13}\text{H}$  and the density  $3.16 \text{ g cm}^{-3}$ .<sup>[24]</sup> These data make it possible to determine both electron density and the contribution to absorption coefficient. Collagen fibrils consist of only light atoms and have a rather complex structure. We believe that they have little effect on the refractive index. The following values of the decrement of refractive index  $\delta$  and the absorption coefficient  $\beta$  were utilized:  $\delta = 2.26 \times 10^{-6}$ ,  $\beta = 3.62 \times 10^{-8}$ . Using the chemical composition and density,  $\delta$  and  $\beta$  can be calculated on the Internet.<sup>[25]</sup> The above values were obtained with a more accurate computer program.<sup>[26]</sup> The computations assumed a point SR source and a detector resolution of  $0.5 \mu\text{m}$ . The consideration of the source size would lead to image averaging at large distances, but we were interested in an ideal situation. The consideration of the detector resolution allowed us to eliminate unobservable fringes.

All our calculations employed the Fast Fourier Transformation (FFT) procedure to calculate the convolution of the Fresnel propagator and the factor containing the transmission function. First, we calculated a direct Fourier transform of the factor, then we multiplied it by the Fourier image of the propagator; and then we calculated the inverse Fourier

transform. The computation was carried out on a set of  $65\,536 = 2^{16}$  points with  $0.01\ \mu\text{m}$  step.

It follows from the above analysis (made for different values of the distance  $Z$ ) that distinguishable changes in the shape of the curves  $I_0^{-1}I(x)$  are observed only for numbers  $N > 100$ , and they slowly increase with increasing  $N$ . At  $N = 50$ , the curves constructed by the two methods practically coincide. Thus one can conclude that the phase-contrast method is quite applicable for the number of voids along the beam of less than 100. At  $N < 100$ , the method gives a good accuracy. It can still be used with lower accuracy at  $100 < N < 200$ , but not at  $N > 200$ . Note that the computation made by the iterative method requires substantially more time.

#### 4. Computer Simulations of 2D Arrays of Tubules in Dentin

Dentin is structured with an array of fluid-containing channels (called dentinal tubules) located in a complex substance. Typically the array of tubules looks like a slightly disordered 2D lattice with a period of  $10\ \mu\text{m}$ , while the diameter of a tubule is about  $4\ \mu\text{m}$ . **Figure 2** shows this structure together with the coordinate axes. As a first approximation, we consider an idealized model of 2D photonic crystal, which represents a strictly periodic 2D system of tubules. One direction is parallel to SR beam propagation direction, the other is normal to the plane in which SR source has its minimum dimensions. As before, the substance is homogeneous along tubules. Therefore, a detector will capture a homogeneous distribution of intensity along tubules.

In fact, in real dentin tubules are not quite parallel to each other. However, it is sufficient if they are parallel within the distance slightly more than the diameter of the first Fresnel zone  $2r_1 = (\lambda z)^{1/2}$ , in which case the change in the structure along the axes of tubules can be neglected. The calculation of the  $50 \times 50$  system of tubules separated by  $10\ \mu\text{m}$  spacing in both directions was carried out at different distances from the specimen using the phase-contrast method. The calculation parameters were the same as in the previous section. The system had the transverse and longitudinal dimension equal to  $500\ \mu\text{m}$ . The dimension of the calculation region was equal to  $655\ \mu\text{m}$ .

**Figure 3** (left panel) shows how the intensity varies in three central periods of  $30\ \mu\text{m}$ , depending on the specimen-to-detector distance from 0 to 50 cm. The transverse dimension of the pattern is  $\approx 20$  times smaller than the dimension of the calculation region. It is interesting that the output wave amplitude is no longer a constant. In the center of the tubules, the amplitude increases by 1.55 times with respect to the points between the tubules. That is, despite the fact that the change in the phase of the wave is very large, there is also a strong amplitude-contrast associated with absorption. In the central part of the tubules, the phase change has a parabolic shape; and the tubules resemble microlenses. The beams are locally focused at the distance that is slightly less than 1 cm, with a maximum intensity value of 5.5 at the focuses. However, in order to better represent the contrast in the entire range of intensities, the values were trimmed from 0.36 (in the minimum) to 3. The estimation of the focal length by the formula of a parabolic

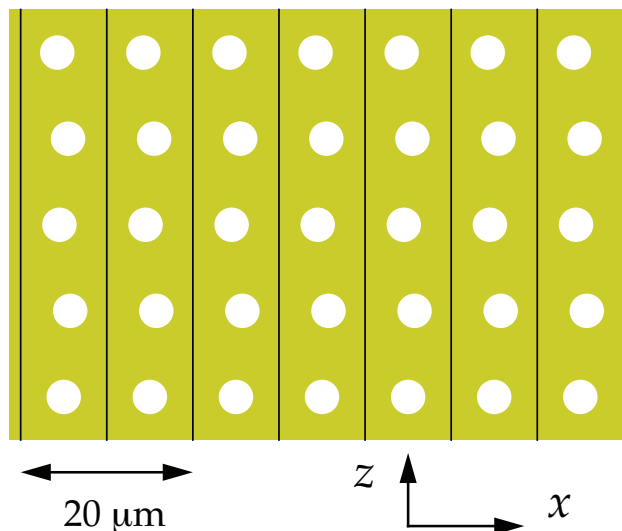


**Figure 2.** Typical arrangement of dentinal tubules considered in computer simulations. The  $z$ -axis lies along the beam, the  $x$ -axis is perpendicular to the beam axis in the plane of high coherence of the beam.

lens<sup>[27]</sup> gives the value  $F = R/2N\delta = 0.88\ \text{cm}$ . After focusing the beams scatter and mix. At some distance interval from 12 to 20 cm maxima of relative intensity appear between the tubules. With increasing distance, the intensity distribution becomes more uniform, remaining periodic. At the distance of 49 cm, the

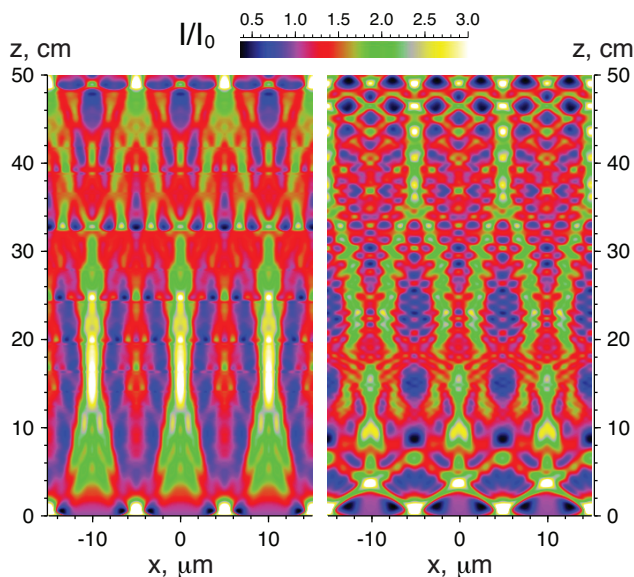


**Figure 3.** The dependence of the relative intensity of the system, which models the dentin structure, on the distance  $z$  from the specimen. The system includes  $50 \times 50$  tubules of a circular cross-section with the diameter of  $4\ \mu\text{m}$ , spaced apart the distance of  $10\ \mu\text{m}$ . Only the central part of the image, which has the size of  $30\ \mu\text{m}$  (3 periods), is shown. Left panel: the structure is a regular lattice. Right panel: the structure contains a weak disorder. See text for details.

maxima are formed again close to the centers of the tubules but of a lower intensity. It should be noted that at times there is a sharp dependence on the distance; that is, on a small distance interval at some values of the distance, the intensity distribution is rapidly rearranged. But there are also such distances at which there are almost no changes. This behavior is difficult to understand, and more research is needed.

It is of interest to model some disorder in the system. Let us consider a system which has 50 periodic chains of tubules with a period of  $p_1 = 10 \mu\text{m}$  in the direction perpendicular to the beam. The distances between the chains in the direction along the beam are equal to  $p = 10 \mu\text{m}$ ; however, the centers of each chain have been displaced in the transverse direction relative to the common center randomly, according to the formula  $Up_1(0.5 - R)$ , where  $R$  is a random number obtained by a random number generator in the interval from 0 to 1. Such distribution of tubules has one parameter  $U$  that can take the values from 0 to 1. At  $U = 0$  we obtain an ideal lattice; at  $U = 1$  we obtain the spread of centers along the entire period. Since in the phase contrast method the phase is summed over all layers along the beam, then the periodicity of the distribution remains; however, the profile of the complex phase inside the period can be arbitrarily complicated. Such system of tubules was generated once, and then it was used unchanged for different distances.

The result of the calculation for  $U = 0.25$  is shown in Figure 3 (right panel). It is seen that even a relatively weak disorder in the system has dramatically changed the intensity distribution in the region behind the focuses. In this case the phase profile is slightly smeared. It deviates from a parabolic shape, however, not strongly, and focusing yet occurs. Then, the maxima between the tubules are quickly formed and, starting from a distance of 2 cm, the intensity distribution does not at all resemble the case of the ordered structure.

The offered interpretation does not address the Talbot theory for the reasons explained below. It is known that after a transmission in free space along the optical path at a distance  $z + z_T$ , the periodic wave field of radiation becomes the same as at a distance  $z$ , where  $z_T = 2p^2/\lambda$ ,  $p$  is the period of the wave field in the transverse direction, and  $\lambda$  is the wavelength.<sup>[28]</sup> This effect is called the Talbot effect. At the distance  $z + z_T/2$ , the wave field will also be the same, but shifted by  $p/2$  in the transverse direction. This means that if the initial wave field has peaks at positions  $-p/2$  and  $p/2$ , then they will appear at positions  $-p, 0, p$  at the distance  $z + z_T/2$ .

Later works (see, e.g., refs. [29,30]) have shown that peaks arise as well at the distances  $z_n = p^2/\lambda n$  with the period of  $p/n$  and the center at 0. This effect is called the fractional Talbot effect. The effect is especially clear if the peaks have a constant phase. If the phase of the wave field within the peaks is variable, then the properties of the wave field transmission in free space become more complex.<sup>[31]</sup>

Our system has the Talbot period equal to  $z_T = 200 \text{ cm}$ . This distance is too long to use in imaging experiments. On the other hand, our system is not completely periodic because its width is only  $50p$ . In addition, the peaks have a variable phase. Therefore, the fractional Talbot effect can be seen approximately for  $n = 2, 3$  (Figure 3), but it is not observed for larger values of  $n$ .

We note that the fractional Talbot effect cannot distort information about the system transverse period, because it takes place in a small interval of  $z$ . Images are always measured at several distances  $z$ , and the real period can be easily seen.

## 5. Conclusion

This investigation was an attempt to explain interference patterns generated by arrays of tubules. The patterns were simulated by using simplified models of dentin material illuminated by coherent synchrotron light. For a single tubular microvoid, the 1D phase-contrast method provides reliable assessment of the cross-sectional area. When the tubule diameters are only a few times smaller than the spacing between them, a tubule array is considered as 2D object. The wave function of radiation within such object is a variable. The consideration of a variable wave function by means of the iterative method shows that for a very thin specimen, the calculation can be carried out by the 2D phase-contrast method without loss of accuracy or information. Although the simulations are accurate enough in this case, no easily explainable patterns emerge from the calculations. One image is not enough to obtain information about the entire structure.

Our computations are still quite far from reality. The problem is too profound and requires further research. Yet, we tried to find whether it is possible to determine a period in the lattice of tubules. We can say with certainty that phase-contrast images allow the determination of the period, which does not fade away even after introducing some long-range disorder into the system with short-range order.

## Conflict of Interest

The authors declare no conflict of interest.

## Keywords

computational physics, dentin, synchrotron radiation phase contrast imaging, voids

Received: May 7, 2018

Revised: July 9, 2018

Published online:

- [1] A. Snigirev, I. Snigireva, V. Kohn, S. Kuznetsov, I. Schelokov, *Rev. Sci. Instrum.* **1995**, *66*, 5486.
- [2] P. Cloetens, R. Barrett, J. Baruchel, J.-P. Guigay, M. Schlenker, *J. Phys. D: Appl. Phys.* **1996**, *29*, 133.
- [3] J.-Y. Buffiere, J. Baruchel, in *Synchrotron Radiation: Basics, Methods and Applications* (Eds: S. Mobilio, F. Boscherini, C. Meneghini), Springer-Verlag, Berlin, Germany **2015**, Ch. 13.
- [4] M. Endrizzi, *Nucl. Instrum. Methods A* **2018**, *878*, 88.
- [5] S. Zabler, P. Cloetens, J.-P. Guigay, J. Baruchel, *Rev. Sci. Instrum.* **2005**, *76*, 073705.
- [6] Ya. I. Nesterets, S. W. Wilkins, T. E. Gureyev, A. Pogany, A. W. Stevenson, *Rev. Sci. Instrum.* **2005**, *76*, 093706.
- [7] S. Zabler, H. Riesemeier, P. Fratzl, P. Zaslansky, *Opt. Express* **2006**, *14*, 8584.

- [8] S. Agliozzo, P. Cloetens, *J. Microscopy* **2004**, 216, 62.
- [9] V. G. Kohn, *Phys. Scr.* **1997**, 56, 14.
- [10] M. Langer, P. Cloetens, J.-P. Guigay, F. Peyrin, *Med. Phys.* **2008**, 35, 4556.
- [11] A. Burvall, U. Lundström, P. A. C. Takman, D. H. Larsson, H. M. Hertz, *Opt. Express* **2011**, 19, 1035910376.
- [12] *X-Ray Tomography in Material Science* (Eds: J. Baruchel, J. Y. Buffière, E. Maire, P. Merle, G. Peix), Hermes, Paris, France **2000**.
- [13] V. G. Kohn, T. S. Argunova, J. H. Je, *Appl. Phys. Lett.* **2007**, 91, 171901.
- [14] V. G. Kohn, T. S. Argunova, J. H. Je, *AIP Adv.* **2013**, 3, 122109.
- [15] V. G. Kohn, T. S. Argunova, J. H. Je, *AIP Adv.* **2014**, 4, 097134.
- [16] V. G. Kohn, T. S. Argunova, J. H. Je, *J. Phys. D: Appl. Phys.* **2010**, 43, 1.
- [17] U. G. K. Wegst, H. Bai, E. Saiz, A. P. Tomsia, R. O. Ritchie, *Nat. Mater.* **2015**, 14, 23.
- [18] R. O. Ritchie, *Nat. Mater.* **2011**, 10, 817.
- [19] I. Zanette, B. Enders, M. Dierolf, P. Thibault, R. Gradl, A. Diaz, M. Guizar-Sicairos, A. Menzel, F. Pfeiffer, P. Zaslansky, *Sci. Rep.* **2015**, 5, 9210.
- [20] J. Takahashi, N. Ohtani, M. Kanaya, *J. Cryst. Growth* **1996**, 167, 596.
- [21] V. G. Kohn, N. V. Tsvigun, *Crystallogr. Rep.* **2014**, 59, 1.
- [22] V. G. Kohn, I. Snigireva, A. Snigirev, *J. Synchrotron Radiat.* **2014**, 21, 729.
- [23] V. G. Kohn, *J. Synchrotron Radiat.* **2018**, 25, 425.
- [24] D. Haverty, S. A. M. Tofail, K. T. Stanton, J. B. McMonagle, *Phys. Rev. B* **2005**, 71, 094103.
- [25] <http://xray-optics.ucoz.ru/js-pro/cir-pro.htm>.
- [26] <http://kohnvict.ucoz.ru/vkacl/vkUtility.htm>.
- [27] A. Snigirev, V. Kohn, I. Snigireva, B. Lengeler, *Nature* **1996**, 384, 49.
- [28] H. F. Talbot, *Philos. Mag.* **1836**, 9, 401.
- [29] M. V. Berry, S. Klein, *J. Mod. Opt.* **1996**, 43, 2139.
- [30] V. G. Kohn, *J. Surf. Invest.: X-ray Synchr. Neutron Techn.* **2016**, 10, 698.
- [31] M. V. Berry, E. Bodenschatz, *J. Mod. Opt.* **1999**, 46, 349.